# From local to critical fluctuations in lattice models:
# A nonperturbative renormalization-group approach

T. Machado and N. Dupuis

*Laboratoire de Physique Théorique de la Matière Condensée, CNRS-UMR 7600, Université Pierre et Marie Curie, 4 Place Jussieu,*
*75252 Paris Cedex 05, France*

We propose an implementation of the nonperturbative renormalization group (NPRG) which applies to lattice models. Contrary to the usual NPRG approach where the initial condition of the RG flow is the mean-field solution, the lattice NPRG uses the (local) limit of decoupled sites as the (initial) reference system. In the long-distance limit, it is equivalent to the usual NPRG formulation and therefore yields identical results for the critical properties. We discuss both a lattice field theory defined on a $d$-dimensional hypercubic lattice and classical spin models. The simplest approximation, the local potential approximation, is sufficient to obtain the critical temperature and the magnetization of the three-dimensional Ising, $XY$, and Heisenberg models to an accuracy on the order of 1%. We show how the local potential approximation can be improved to include a nonzero anomalous dimension $\eta$ and discuss the Berezinskii-Kosterlitz-Thouless transition of the two-dimensional $XY$ model on a square lattice.

## I. INTRODUCTION

Many models of statistical physics and condensed matter are defined on a lattice. The phase diagram of a lattice model usually depends on the lattice type, the range and strength of interactions, as well as other details of the Hamiltonian. On the other hand, the precise knowledge of the Hamiltonian is often not necessary to understand the long-distance behavior of the system, in particular the universal critical properties near a second-order phase transition. In this paper, we describe an approach based on the nonperturbative renormalization group (NPRG) which captures both local and critical fluctuations in lattice models and therefore describes universal and nonuniversal properties. In particular, we can calculate the critical exponents, the transition temperature, and the magnetization in classical spin models.

The NPRG approach has been successfully applied to many areas of physics and in particular to the study of critical phenomena [1–3]. It has recently been extended to lattice models [4]. The strategy of the NPRG is to build a family of models indexed by a momentum scale parameter $k$, such that fluctuations are smoothly taken into account as $k$ is lowered from a microscopic scale $\Lambda$ down to 0. In practice, this is achieved by adding to the Hamiltonian (or the action) a "regulator" term $\Delta H_k$, which vanishes for $k=0$, and computing the corresponding Gibbs free energy (or effective action in the field theory terminology) $\Gamma_k$. The initial value $\Delta H_\Lambda$ is chosen such that in the reference system defined by the Hamiltonian $H+\Delta H_\Lambda$ all fluctuations are effectively frozen. The determination of $\Gamma_\Lambda$ is then reduced to a saddle-point (mean-field) calculation. The Gibbs free energy $\Gamma_{k=0}$ we are eventually interested in is obtained from that of the reference system by solving a RG flow equation. The latter cannot in general be solved exactly (even numerically) and one has to resort to some approximations. The approximate flow equation must be sufficiently accurate (and yet tractable) to provide a good approximation of the state of the system.

In some cases, however, the mean-field solution is too far away from the actual state of the system to provide a reliable initial condition for the NPRG procedure. An example is provided by the localization transition between a Mott insulator and a superfluid in lattice boson systems. The two-pole structure of the local (on-site) propagator is crucial for the very existence of the transition. This structure is however impossible to reproduce using a RG approach starting from the mean-field (Bogoliubov) approximation. This prevents a straightforward generalization of recent NPRG studies of interacting bosons [5–11] to lattice models such as the Bose-Hubbard model.

We therefore propose a NPRG scheme for lattice models where the reference system corresponds to the (local) limit of decoupled sites. As an expansion about the local limit, the lattice NPRG is reminiscent of Kadanoff's idea of block spins [12], although the way intersite interactions are progressively introduced when lowering the momentum scale $k$ makes it significantly different from a real-space RG. In the long-distance limit, the lattice NPRG is equivalent to the usual NPRG formulation and therefore yields identical results for the critical properties.

The possibility to start from a reference system which already includes short-range fluctuations has been recognized before and was used by Parola and Reatto in the hierarchical reference theory (HRT) of fluids [13], an approach which bears many similarities with the lattice NPRG. An important aspect of the lattice NPRG is that it is formulated in the field theory language commonly used in the NPRG approach. Its relation to the standard NPRG formulation is therefore obvious, and many of the approximate solutions of the flow equation satisfied by $\Gamma_k$ proposed previously also apply to the lattice case.

In Sec. II we introduce the lattice NPRG for a lattice field theory. We first recall the "standard" NPRG approach to lattice models [4] and then show that the lattice NPRG scheme merely results from a different initial condition while the long-distance (small $k$) behavior of the effective action $\Gamma_k$ remains the same. As an application, we derive a lattice field theory from the Ising model and compute the transition tem-

perature in the local potential approximation (LPA). In Sec. III, we apply the lattice NPRG to classical spin models without deriving first a lattice field theory. We find that the LPA is sufficient to obtain the critical temperature and the magnetization of the three-dimensional (3D) Ising, *XY*, and Heisenberg models to an accuracy on the order of 1%. We also discuss an improvement of the LPA (known as the LPA′) which yields a nonzero anomalous dimension $\eta$. In Sec. IV, we use the lattice NPRG to calculate the Berezinskii-Kosterlitz-Thouless (BKT) [14,15] transition temperature of the two-dimensional (2D) *XY* model on a square lattice.

## II. LATTICE NONPERTURBATIVE RG

We consider a lattice field theory defined on a *d*-dimensional hypercubic lattice,

$$H[\varphi] = \frac{1}{2}\sum_{\mathbf{q}} \varphi_{-\mathbf{q}}\epsilon_0(\mathbf{q})\varphi_{\mathbf{q}} + \sum_{\mathbf{r}} U_0(\varphi_{\mathbf{r}}), \qquad (1)$$

where {$\mathbf{r}$} denotes the $N$ sites of the lattice. For simplicity, we consider a one-component real field $\varphi_{\mathbf{r}}$. $\varphi_{\mathbf{q}} = N^{-1/2}\sum_{\mathbf{r}} e^{-i\mathbf{q}\cdot\mathbf{r}}\varphi_{\mathbf{r}}$ is the Fourier-transformed field. The momentum $\mathbf{q}$ is restricted to the first Brillouin zone $]-\pi,\pi]^d$ of the reciprocal lattice. In the thermodynamic limit ($N\to\infty$),

$$\frac{1}{N}\sum_{\mathbf{q}} \to \int_{-\pi}^{\pi}\frac{dq_1}{2\pi}\cdots\int_{-\pi}^{\pi}\frac{dq_d}{2\pi} \equiv \int_{\mathbf{q}}. \qquad (2)$$

The potential $U_0$ is defined such that $\epsilon_0(\mathbf{q}=0)=0$ but is otherwise arbitrary. $\epsilon_0(\mathbf{q})\simeq\epsilon_0\mathbf{q}^2$ for $\mathbf{q}\to 0$ and $\max_{\mathbf{q}}\epsilon_0(\mathbf{q})=\epsilon_0^{\max}$. The lattice spacing is taken as the unit length.

To implement the renormalization-group (RG) procedure, we add to Hamiltonian (1) the regulator term

$$\Delta H_k[\varphi] = \frac{1}{2}\sum_{\mathbf{q}} \varphi_{-\mathbf{q}}R_k(\mathbf{q})\varphi_{\mathbf{q}}. \qquad (3)$$

Throughout the paper, we take

$$R_k(\mathbf{q}) = [\epsilon_k - \epsilon_0(\mathbf{q})]\theta[\epsilon_k - \epsilon_0(\mathbf{q})] \qquad (4)$$

($\epsilon_k = \epsilon_0 k^2$), which is adapted from Ref. [16] to the lattice case. The cutoff function $R_k(\mathbf{q})$ leaves the high-momentum modes $[\epsilon_0(\mathbf{q})>\epsilon_k]$ unaffected and gives a mass $\epsilon_k$ to the low-energy ones [their effective (bare) dispersion satisfies $\epsilon_0(\mathbf{q})+R_k(\mathbf{q})=\epsilon_k$].

In the presence of an external field, the partition function reads

$$Z_k[h] = \int \mathcal{D}[\varphi]\exp\left(-H[\varphi] - \Delta H_k[\varphi] + \sum_{\mathbf{r}} h_{\mathbf{r}}\varphi_{\mathbf{r}}\right) \qquad (5)$$

and the order parameter is given by

$$\phi_{\mathbf{r}} = \langle\varphi_{\mathbf{r}}\rangle = \frac{\partial \ln Z_k[h]}{\partial h_{\mathbf{r}}}. \qquad (6)$$
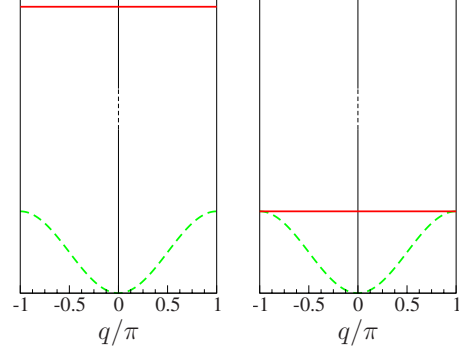
The so-called average effective action,



FIG. 1. (Color online) Initial effective dispersion $\epsilon_0(q)+R_k(q)$ in the standard (left panel) and lattice (right panel) NPRG schemes [$d=1$ and $\epsilon_0(q)=2\epsilon_0(1-\cos q)$]. The green dashed line shows the bare dispersion $\epsilon_0(q)$.

$$\Gamma_k[\phi] = -\ln Z_k[h] + \sum_{\mathbf{r}} h_{\mathbf{r}}\phi_{\mathbf{r}} - \Delta H_k[\phi], \qquad (7)$$

is defined as a modified Legendre transform which includes the explicit subtraction of $\Delta H_k[\phi]$ [2]. It satisfies the exact flow equation [1],

$$\partial_k\Gamma_k[\phi] = \frac{1}{2}\sum_{\mathbf{q}} \partial_k R_k(\mathbf{q})(\Gamma_k^{(2)}[\phi] + R_k)^{-1}_{\mathbf{q},-\mathbf{q}} \qquad (8)$$

as the energy scale $\epsilon_k$ is varied. $\Gamma_k^{(2)}[\phi]$ is the second-order functional derivative of $\Gamma_k[\phi]$. Since $R_{k=0}(\mathbf{q})=0$, $\Gamma_{k=0}[\phi]$ coincides with the effective action of original model (1).

### A. Standard NPRG scheme

In the standard NPRG approach to lattice models [4], the initial value $\Lambda$ of the momentum scale $k$ is chosen such that $\epsilon_\Lambda$ is much larger than all characteristic energy scales of the problem. In this limit, all fluctuations are frozen and mean-field theory becomes exact: $\Gamma_\Lambda[\phi]=H[\phi]$. The first part of the RG procedure when $\epsilon_k$ varies between $\epsilon_\Lambda$ and $\epsilon_{k_{\mathrm{in}}} = \epsilon_0^{\max}$ is purely local since the effective (bare) dispersion $\epsilon_0(\mathbf{q})+R_k(\mathbf{q})=\epsilon_k$ remains dispersionless for all modes. Only for $k<k_{\mathrm{in}}$ does the intersite coupling start to play a role. When $k\ll 1$, i.e., when $1/k$ is much larger than the lattice spacing, the lattice does not matter any more. This result is a direct consequence of the structure of the flow equation; the $\partial_k R_k$ term in Eq. (8) implies that only modes with $|\mathbf{q}|\lesssim k$ contributes to $\partial_k\Gamma_k$. When $k\ll 1$, one can therefore approximate $\epsilon_0(\mathbf{q})\simeq\epsilon_0\mathbf{q}^2$, and one recovers the flow equation of the continuum model obtained from Eqs. (1) and (3) by replacing $\epsilon_0(\mathbf{q})$ by $\epsilon_0\mathbf{q}^2$ [4].

### B. Lattice NPRG scheme

In the lattice NPRG, we start the RG procedure from $k=k_{\mathrm{in}}$; i.e., we bypass the initial stage of the flow $k_{\mathrm{in}}\leq k\leq\Lambda$ where the fluctuations are purely local (Fig. 1). The average effective action $\Gamma_{k_{\mathrm{in}}}[\phi]$ is no longer given by the microscopic Hamiltonian $H[\phi]$ (since the mean-field solution is not exact for the Hamiltonian $H+\Delta H_{k_{\mathrm{in}}}$) but its com-
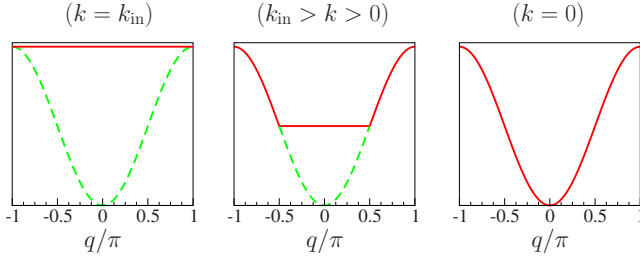
FIG. 2. (Color online) Effective (bare) dispersion $\epsilon_0(q)+R_k(q)$ for $k=k_{\text{in}}$, $k_{\text{in}}>k>0$, and $k=0$ with cutoff function (4) [$d=1$ and $\epsilon_0(q)=2\epsilon_0(1-\cos q)$]. The green dashed line shows the bare dispersion $\epsilon_0(q)$.

putation reduces to a single-site problem which can be easily solved numerically (and even analytically in some models). In principle, the NPRG scheme can be defined with any cutoff function provided that the latter satisfies the initial condition [17]

$$R_{k_{\text{in}}}(\mathbf{q}) = -\epsilon_0(\mathbf{q}) + C, \qquad (9)$$

ensuring that the sites are decoupled (the limit $C\to\infty$ corresponding to the standard scheme). The choice $C=\epsilon_{k_{\text{in}}}=\epsilon_0^{\max}$ made in Eq. (4) is however very natural since it allows to set up the RG procedure for $k<k_{\text{in}}$ in the usual way, i.e., by modifying the (bare) dispersion of the low-energy modes $\epsilon_0(\mathbf{q})<\epsilon_k$ without affecting the high-energy modes (Fig. 2).

For $k_{\text{in}}>k>0$, the effective coupling in real space [defined as the Fourier transform of $\epsilon_0(\mathbf{q})+R_k(\mathbf{q})$] is long range and oscillating. The oscillating part comes from the behavior of $R_k(\mathbf{q})$ for $\epsilon_0(\mathbf{q})\sim\epsilon_k$. Although the lattice NPRG is based on an expansion about the local limit, it markedly differs from Kadanoff's real-space RG [12] in the way degrees of freedom are progressively integrated out.

The standard and lattice NPRG schemes thus differ only in the initial condition. Both schemes are equivalent for $k\leq k_{\text{in}}$ when the flow Eq. (8) is solved exactly for $k>k_{\text{in}}$ in the standard scheme. As shown in Sec. II C, this is the case for classical models even within simple approximations. In practice, however, one often relies on an approximate solution of the flow equation. The NPRG lattice scheme is preferable whenever the (approximate) flow equation gives a poor description of $\Gamma_{k_{\text{in}}}[\phi]$ starting from the mean-field result $\Gamma_\Lambda[\phi]=H[\phi]$. As discussed in Sec. I, this is to be expected in quantum models [such as the (Bose-)Hubbard model] where on-site (quantum) fluctuations make the local limit nontrivial. Finally, we point out another advantage of the lattice NPRG; it enables to study classical spin models without first deriving a field theory (see Sec. III).

## C. Application to the Ising model

We consider the Ising model

$$H = -J\beta\sum_{\langle\mathbf{r},\mathbf{r}'\rangle} S_{\mathbf{r}}S_{\mathbf{r}'} \quad (S_{\mathbf{r}}=\pm 1) \qquad (10)$$

defined on a $d$-dimensional hypercubic lattice ($\beta=1/T$). $\langle\mathbf{r},\mathbf{r}'\rangle$ denotes nearest-neighbor sites. To apply the NPRG

approach, one possibility is to first derive a field theory (another, more natural, approach is described in Sec. III). To this end, one considers the Hamiltonian

$$H_\mu = -J\beta\sum_{\langle\mathbf{r},\mathbf{r}'\rangle} S_{\mathbf{r}}S_{\mathbf{r}'} - \mu\beta\sum_{\mathbf{r}} S_{\mathbf{r}}^2 \equiv -\frac{1}{2}\sum_{\mathbf{r},\mathbf{r}'} S_{\mathbf{r}}A_{\mathbf{r},\mathbf{r}'}^{(\mu)}S_{\mathbf{r}'}, \qquad (11)$$

which differs from that of the Ising model only by the additive constant $-\mu\beta N$. The matrix $A^{(\mu)}$ is diagonal in Fourier space with eigenvalues

$$\lambda_\mu(\mathbf{q}) = 2\beta\left(J\sum_{\nu=1}^{d}\cos q_\nu + \mu\right). \qquad (12)$$

For $\mu>Jd$ the matrix $A^{(\mu)}$ is positive [$\lambda_\mu(\mathbf{q})>0 \quad \forall \; \mathbf{q}$] and can be inverted. We can then rewrite the partition function of the Ising model using a Hubbard-Stratonovich transformation,

$$Z_\mu \propto \sum_{\{S_{\mathbf{r}}\}}\int_{-\infty}^{\infty}\prod_{\mathbf{r}}d\varphi_{\mathbf{r}}\exp\left(-\frac{1}{2}\sum_{\mathbf{r},\mathbf{r}'}\varphi_{\mathbf{r}}A_{\mathbf{r},\mathbf{r}'}^{(\mu)-1}\varphi_{\mathbf{r}'}+\sum_{\mathbf{r}}\varphi_{\mathbf{r}}S_{\mathbf{r}}\right)$$

$$\propto \int_{-\infty}^{\infty}\prod_{\mathbf{r}}d\varphi_{\mathbf{r}}\exp\left(-\frac{1}{2}\sum_{\mathbf{r},\mathbf{r}'}\varphi_{\mathbf{r}}A_{\mathbf{r},\mathbf{r}'}^{(\mu)-1}\varphi_{\mathbf{r}'}+\sum_{\mathbf{r}}\ln\cosh\varphi_{\mathbf{r}}\right). \qquad (13)$$

We thus obtain a lattice field theory with the Hamiltonian

$$H_\mu[\varphi] = \frac{1}{2}\sum_{\mathbf{q}}\varphi_{-\mathbf{q}}\left[\frac{1}{\lambda_\mu(\mathbf{q})}-\frac{1}{\lambda_\mu(0)}\right]\varphi_{\mathbf{q}}$$

$$+ \sum_{\mathbf{r}}\left[\frac{\varphi_{\mathbf{r}}^2}{2\lambda_\mu(0)}-\ln\cosh\varphi_{\mathbf{r}}\right]. \qquad (14)$$

Rescaling the field, we can cast the Hamiltonian in form (1) with

$$\epsilon_0(\mathbf{q}) = 2d(Jd+\mu)\frac{1-\gamma_{\mathbf{q}}}{Jd\gamma_{\mathbf{q}}+\mu},$$

$$U_0(\varphi) = \frac{Jd+\mu}{J}\varphi^2 - \ln\cosh\left(2\sqrt{\frac{\beta}{J}}(Jd+\mu)\varphi\right) \qquad (15)$$

($\gamma_{\mathbf{q}}=d^{-1}\sum_\nu\cos q_\nu$). The (bare) dispersion $\epsilon_0(\mathbf{q})$ includes long-range interactions and $\epsilon_0(\pi,\pi,\ldots)=\epsilon_0^{\max}$ diverges for $\mu\to Jd$. In the limit $\mu\to\infty$ long-range interactions are suppressed and $\epsilon_0(\mathbf{q})\to 2d(1-\gamma_{\mathbf{q}})$.

We are now in a position to apply the NPRG approach. In the standard scheme (Sec. II A), the initial value $\Gamma_\Lambda[\phi]=H[\phi]$ of the effective action is defined by Hamiltonian (1), with $\epsilon_0(\mathbf{q})$ and $U_0$ given by Eq. (15). In the lattice NPRG scheme, the initial value $U_{k_{\text{in}}}$ of the effective potential has to be computed numerically. One has $Z_{k_{\text{in}}}[h]=\prod_{\mathbf{r}}z_{k_{\text{in}}}(h_{\mathbf{r}})$, where
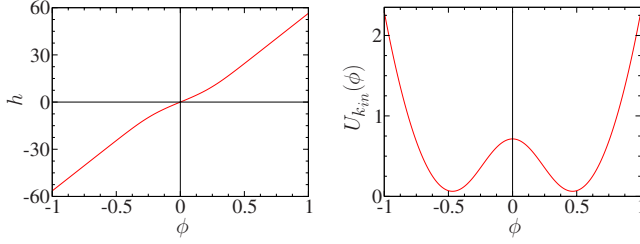
FIG. 3. (Color online) Left panel: function $h(\phi)$ obtained from the numerical solution of Eq. (17). Right panel: effective potential $U_{k_{in}}(\phi)$ [Eq. (19)]. $\mu=5$, $T=4.48J$, and $d=3$.

$$z_{k_{in}}(h) = \int_{-\infty}^{\infty} d\varphi \, e^{-(1/2)\epsilon_{k_{in}}\varphi^2 - U_0(\varphi) + h\varphi} \qquad (16)$$

is the partition function of a single site in an external field $h$. The relation between $\phi_\mathbf{r}$ and $h_\mathbf{r}$ is obtained from the equation

$$\phi_\mathbf{r} = \frac{\partial}{\partial h_\mathbf{r}} \ln z_{k_{in}}(h_\mathbf{r}), \qquad (17)$$

which has to be computed and inverted numerically (Fig. 3). The initial value of the average effective action then takes the form

$$\Gamma_{k_{in}}[\phi] = -\sum_\mathbf{r} \ln z_{k_{in}}(h_\mathbf{r}) + \sum_\mathbf{r} h_\mathbf{r}\phi_\mathbf{r} - \Delta H_{k_{in}}[\phi]$$

$$= \sum_\mathbf{r} U_{k_{in}}(\phi_\mathbf{r}) + \frac{1}{2}\sum_\mathbf{q} \phi_{-\mathbf{q}}\epsilon_0(\mathbf{q})\phi_\mathbf{q}, \qquad (18)$$

where

$$U_{k_{in}}(\phi) = \frac{1}{N}\Gamma_{k_{in}}[\phi]\big|_{\phi_\mathbf{r}=\phi} = -\ln z_{k_{in}}(h) + h\phi - \frac{\epsilon_{k_{in}}}{2}\phi^2 \qquad (19)$$

is the effective potential (Fig. 3).

In the LPA, one neglects the $k$ dependence of the dispersion so that

$$\Gamma_k[\phi] = \sum_\mathbf{r} U_k(\rho_\mathbf{r}) + \frac{1}{2}\sum_\mathbf{q} \phi_{-\mathbf{q}}\epsilon_0(\mathbf{q})\phi_\mathbf{q}. \qquad (20)$$

Here and in the following, we consider $U_k$ as a function of $\rho_\mathbf{r} = \phi_\mathbf{r}^2/2$. From Eq. (8), one deduces

$$\partial_k U_k(\rho) = \frac{1}{2}\int_\mathbf{q} \frac{\partial_k R_k(\mathbf{q})}{\epsilon_0(\mathbf{q}) + R_k(\mathbf{q}) + U_k'(\rho) + 2\rho U_k''(\rho)}. \qquad (21)$$

With cutoff function (4), Eq. (21) is reduced to

$$k\partial_k U_k(\rho) = \frac{\epsilon_k}{\epsilon_k + U_k'(\rho) + 2\rho U_k''(\rho)}\int_\mathbf{q} \theta[\epsilon_k - \epsilon_0(\mathbf{q})]. \qquad (22)$$

The integral over $\mathbf{q}$ can be rewritten as

$$\int_\mathbf{q} \theta[\epsilon_k - \epsilon_0(\mathbf{q})] = \int_0^{\epsilon_k} d\epsilon \mathcal{D}(\epsilon), \qquad (23)$$
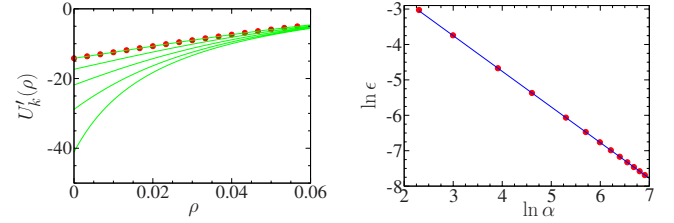


FIG. 4. (Color online) Left panel: derivative $U_k'(\rho)$ of the effective potential for various values of $k$ ranging from $\Lambda$ to $k_{in}$. The initial value $U_\Lambda(\rho) = U_0(\rho)$ is given by Eq. (15). The red points show the solution $U_{k_{in}}'(\rho)$ directly obtained from a numerical solution of the single-site partition function $z_{k_{in}}(h)$ [Eq. (16)]. Right panel: relative error $\epsilon$ vs $\alpha = (\Lambda/k_{in})^2$. $\mu=5$, $T=4.48J$, and $d=3$.

where [18]

$$\mathcal{D}(\epsilon) = \int_\mathbf{q} \delta[\epsilon - \epsilon_0(\mathbf{q})]. \qquad (24)$$

In the local fluctuation regime $k_{in} \leq k \leq \Lambda$, $H[\varphi] + \Delta H_k[\varphi]$ is a local Hamiltonian (no intersite coupling). It follows that both $-\ln Z_k[h]$ and its Legendre transform reduce to a sum of single-site contributions. The LPA for the average effective action $\Gamma_k[\phi]$ is therefore exact. We have computed the derivative $U_k'$ of the effective potential for various values of $\alpha = \epsilon_\Lambda/\epsilon_0^{max} = (\Lambda/k_{in})^2$. (In practice, it is easier to solve for $U_k'$ than $U_k$.) The results are shown in Fig. 4 for $\alpha = 1000$ (we comment on the numerical method in Sec. III A). As $k$ decreases from $\Lambda$ to $k_{in}$, the potential $U_k'(\rho)$ converges toward the exact solution obtained from the numerical computation of the local partition function $z_{k_{in}}(h)$ [Eqs. (16) and (19)]. The relative error is shown in the right panel of Fig. 4. It decreases as $1/\alpha$, in agreement with the fact that the validity of the mean-field (saddle-point) approximation to $Z_\Lambda[h]$ for large $\Lambda$ is controlled by $R_\Lambda^{-1} \sim \epsilon_\Lambda^{-1} \sim \alpha^{-1}$. We therefore conclude that the standard and lattice NPRG schemes are equivalent in the LPA for classical lattice field theories.

The critical temperature is obtained from the divergence of the susceptibility $\chi = 1/U_{k=0}'(\rho=0)$ (or, equivalently, the divergence of the correlation length $\xi = \sqrt{\chi}$) [19]. For $\alpha = 1000$ and $d=3$ one finds that $T_c \simeq 0.747 T_c^{MF}$ is independent of $\mu$ and in very good agreement with the "exact" result $T_c^{exact} \simeq 0.752 T_c^{MF}$ obtained from the Monte Carlo simulations [20].

## III. CLASSICAL SPIN MODELS

In this section, we show that the lattice NPRG can be applied to classical spin models without first deriving a field theory. For simplicity, we consider the Ising model on a $d$-dimensional hypercubic lattice [Eq. (10)]. In the presence of an external field and a regulator term $\Delta H_k$, the partition function reads

$$Z_k[h] = \sum_{\{S_\mathbf{r}\}} \exp\left( \frac{J}{T}\sum_{\langle \mathbf{r},\mathbf{r}'\rangle} S_\mathbf{r}S_{\mathbf{r}'} - \frac{1}{2}\sum_{\mathbf{r},\mathbf{r}'} S_\mathbf{r}R_k(\mathbf{r},\mathbf{r}')S_{\mathbf{r}'} + \sum_\mathbf{r} h_\mathbf{r}S_\mathbf{r}\right) = \sum_{\{S_\mathbf{r}\}} \exp\left( -\frac{1}{2}\sum_\mathbf{q} S_{-\mathbf{q}}[\epsilon_0(\mathbf{q}) - 2\epsilon_0 d + R_k(\mathbf{q})]S_\mathbf{q} + \sum_\mathbf{r} h_\mathbf{r}S_\mathbf{r}\right),$$

$$(25)$$

where

$$\epsilon_0(\mathbf{q}) = 2\epsilon_0 \sum_{\nu=1}^{d}(1 - \cos q_\nu), \tag{26}$$

with $\epsilon_0 = J/T$. Since $S_\mathbf{r}^2 = 1$, the term $2d\epsilon_0$ in Eq. (25) contributes a constant term to the Hamiltonian and can be omitted. The magnetization at site $\mathbf{r}$ is given by

$$m_\mathbf{r} = \langle S_\mathbf{r}\rangle = \frac{\partial \ln Z_k[h]}{\partial h_\mathbf{r}} \tag{27}$$

and the average effective action is defined by

$$\Gamma_k[m] = -\ln Z_k[h] + \sum_\mathbf{r} h_\mathbf{r}m_\mathbf{r} - \Delta H_k[m]. \tag{28}$$

The standard NPRG scheme cannot be used since the partition function is not expressed as a functional integral over a continuous variable. A regulator term $\epsilon_k\Sigma_\mathbf{q}S_{-\mathbf{q}}S_\mathbf{q} = \epsilon_k\Sigma_\mathbf{r}S_\mathbf{r}^2 = N\epsilon_k$ would only add a constant term to the Hamiltonian. On the contrary, there is no difficulty to apply the lattice NPRG scheme. With cutoff function (4), one has

$$Z_{k_{\mathrm{in}}}[h] = \sum_{\{S_\mathbf{r}\}} \exp\left( -2d\epsilon_0 N + \sum_\mathbf{r} h_\mathbf{r}S_\mathbf{r}\right) = e^{-2d\epsilon_0 N}\prod_\mathbf{r} z(h_\mathbf{r}),$$

$$(29)$$

where

$$z(h) = \sum_{S=\pm 1} e^{hS} = 2\cosh(h) \tag{30}$$

is the partition function of a single site in an external field $h$. The magnetization at site $\mathbf{r}$,

$$m_\mathbf{r} = \frac{\partial}{\partial h_\mathbf{r}}\ln z(h_\mathbf{r}) = \tanh(h_\mathbf{r}), \tag{31}$$

varies between $-1$ and $1$. Up to an additive constant, we obtain

$$\Gamma_{k_{\mathrm{in}}}[m] = \sum_\mathbf{r} U_{k_{\mathrm{in}}}(\rho_\mathbf{r}) + \frac{1}{2}\sum_\mathbf{q} m_{-\mathbf{q}}\epsilon_0(\mathbf{q})m_\mathbf{q} \tag{32}$$

and the effective potential [21]

$$U_{k_{\mathrm{in}}}(\rho) = \frac{1}{2}\ln(1 - 2\rho) + \sqrt{2\rho}\,\mathrm{argtanh}(\sqrt{2\rho}) - 4d\epsilon_0\rho,$$

$$(33)$$

where $\rho_\mathbf{r} = m_\mathbf{r}^2/2$. $U_{k_{\mathrm{in}}}(1/2) = \ln(2) - 2d\epsilon_0$ is finite but $U'_{k_{\mathrm{in}}}(\rho) \sim -\frac{1}{2}\ln(1 - 2\rho)$ diverges for $\rho \to 1/2$. This divergence suppresses the propagator

$$\frac{1}{\epsilon_k + R_k(\mathbf{q}) + U'_k(\rho) + 2\rho U'_k(\rho)} \tag{34}$$

appearing in the flow [Eq. (21)] and therefore the fluctuations corresponding to a large magnetization.

A comment is in order here. We have followed the usual convention to define the average effective action $\Gamma_k$ as a modified Legendre transform which includes the explicit subtraction of $\Delta H_k[m]$ [Eq. (7)] [2]. The definition of the average effective action $\Gamma_k$ is of course arbitrary provided that $\Gamma_{k=0}$ corresponds to the true Legendre transform of the original model. Since

$$U_{k_{\mathrm{in}}}(\rho) = \rho(1 - 4d\epsilon_0) + \mathcal{O}(\rho^2) \tag{35}$$

for $\rho \to 0$, we find that the initial transition temperature is determined by $1 = 4d\epsilon_0$, i.e., $T_c^{(k_{\mathrm{in}})} = 4dJ$, which differs from the mean-field transition temperature $T_c^{\mathrm{MF}} = 2dJ$ by a factor of 2. $\Gamma_{k_{\mathrm{in}}}[m]$ assumes a mean-field treatment of the intersite coupling term $\frac{1}{2}\Sigma_\mathbf{q}S_{-\mathbf{q}}\epsilon_0(\mathbf{q})S_\mathbf{q}$ as in the usual mean-field approach to the Ising model. The discrepancy between $T_c^{(k_{\mathrm{in}})}$ and $T_c^{\mathrm{MF}}$ comes from the fact that $\frac{1}{2}\Sigma_\mathbf{q}S_{-\mathbf{q}}\epsilon_0(\mathbf{q})S_\mathbf{q}$ includes a local term $\frac{1}{2}\Sigma_\mathbf{r}2d\epsilon_0 S_\mathbf{r}^2 = Nd\epsilon_0$. The latter contributes a mere constant to the Hamiltonian but is considered at the mean-field level in the average effective action where it gives a term $-d\epsilon_0\Sigma_\mathbf{r}m_\mathbf{r}^2$. To make contact with the usual mean-field theory, we consider the average effective action

$$\bar{\Gamma}_k[m] = \Gamma_k[m] + \frac{1}{2}\sum_\mathbf{r} R_k(\mathbf{r},\mathbf{r})m_\mathbf{r}^2 \tag{36}$$

and the corresponding effective potential

$$\bar{U}_k(\rho) = U_k(\rho) + \rho R_k(\mathbf{r},\mathbf{r}). \tag{37}$$

$\bar{\Gamma}_k[m]$ differs from the true Legendre transform only by nonlocal terms. The initial value

$$\bar{U}_{k_{\mathrm{in}}}(\rho) = \rho(1 - 2d\epsilon_0) + \mathcal{O}(\rho^2) \tag{38}$$

reproduces the mean-field result $T_c^{(k_{\mathrm{in}})} = T_c^{\mathrm{MF}}$. Again we stress that $\Gamma_k$ and $\bar{\Gamma}_k$ lead to the same $k=0$ results and in particular to the same critical temperature.

### A. Local Potential Approximation

We have solved the equation for $U'_k(\rho)$ [see Eq. (22)] numerically using Euler's method with a typical RG time step $\Delta t = -10^{-4}$ [$t = \ln(k/k_{\mathrm{in}})$]. The function $U'_k(\rho)$ is discretized with a few hundreds points in $\rho$. The convexity of the potential (see Fig. 6) makes the numerical resolution difficult below $T_c$ (in particular at low temperatures) and there

TABLE I. Critical temperature $T_c^{\mathrm{NPRG}}$ obtained in the LPA compared to the mean-field estimate $T_c^{\mathrm{MF}}$ and the Monte Carlo result $T_c^{\mathrm{exact}}$ [20,22,23]. All temperatures are in unit of $J$.

|  | $T_c^{\mathrm{MF}}$ | $T_c^{\mathrm{exact}}$ | $T_c^{\mathrm{NPRG}}$ |
|---|---|---|---|
| Ising 3D | 6 | 4.51 | 4.48 |
| $XY$ 3D | 3 | 2.20 | 2.18 |
| Heisenberg 3D | 2 | 1.44 | 1.42 |

is a tendency to numerical instability for large values of $|t|$. However, the value $\rho_0$ for which $U_k'(\rho) = 0$ usually converges before instability problems arise.

The critical temperature is obtained from the criterion $U_{k=0}'(\rho=0) = 0$ (Sec. II C). One finds $T_c \simeq 0.747 T_c^{\mathrm{MF}}$ for the three-dimensional Ising model, in very good agreement with the results of Sec. II C and the exact result $T_c^{\mathrm{exact}} \simeq 0.752 T_c^{\mathrm{MF}}$ obtained from the Monte Carlo simulations [20]. We have obtained a similar accuracy for the critical temperature of the $XY$ and Heisenberg models in $d=3$ (Table I).

Figure 5 shows the transition temperature $T_c^{(k)}$ of the three-dimensional Ising model deduced from the effective potentials $U_k$ and $\bar{U}_k$ [Eq. (37)]. As $k$ decreases, $T_c^{(k)}$ converges rapidly toward the actual transition temperature $T_c = T_c^{(k=0)}$. This result is due to the fact that all degrees of freedom contribute more or less equally to the thermodynamics. Once $k \ll k_{\mathrm{in}}$, thermodynamic quantities are therefore obtained with a reasonable accuracy. This also explains why the LPA, which does not correctly describe the long-distance limit of the propagator when $T \simeq T_c$, is remarkably successful in computing the transition temperature and other thermodynamic quantities.

Figure 6 shows the derivative $U_k'(\rho)$ of the effective potential for $k = k_{\mathrm{in}}$ and $k=0$ at criticality ($T = 0.747 T_c^{\mathrm{MF}}$), as well as $U_{k=0}'(\rho)$ for $T = T_c$, $T > T_c$, and $T < T_c$. In the latter case, we find $U_{k=0}'(\rho) = 0$ and therefore $U_{k=0}(\rho) = \mathrm{const}$ for $\rho \leq \rho_0$, where $\rho_0 = m_0^2/2$ determines the actual magnetization $m_0$ of the system. This result is a consequence of the convexity of the potential in the low-temperature phase, a property which is known to be satisfied in the LPA [2].

In Fig. 7, we show the uniform susceptibility $\chi = 1/U_{k=0}'(\rho=0)$ in the high-temperature phase [19], as well as the magnetization below $T_c$ with the Essam-Fisher



FIG. 6. (Color online) Left panel: potentials $U_{k=0}'(\rho)$ (red solid line) and $U_{k_{\mathrm{in}}}'(\rho)$ (green dashed line) at criticality ($T = T_c$) in the LPA ($d=3$). Right panel: potential $U_{k=0}'(\rho)$ for $T = T_c$ (red dotted line), $T = 1.05 T_c$ (green dashed line), and $T = 0.95 T_c$ (blue solid line).

approximant [24]. We find the critical exponents $\nu = 2\beta = \gamma/2 \simeq 0.64 - 0.65$ (with $\eta = 0$ in the LPA), in agreement with the known result in the LPA with cutoff function (4) [16,25].

Not surprisingly, the LPA is not as accurate in two dimensions. For the 2D Ising model, we find $T_c \simeq 0.48 T_c^{\mathrm{MF}}$, to be compared with the exact result $T_c^{\mathrm{exact}} = 2J/\ln(1+\sqrt{2}) \simeq 0.567 T_c^{\mathrm{MF}}$ [26].

### B. Renormalization of the spectrum

A natural generalization of the LPA includes a renormalization of the amplitude of the spectrum. We therefore consider the ansatz

$$\Gamma_k[m] = \sum_{\mathbf{r}} U_k(\rho_{\mathbf{r}}) + \frac{1}{2}\sum_{\mathbf{q}} A_k \epsilon_0(\mathbf{q}) m_{-\mathbf{q}} m_{\mathbf{q}}. \quad (39)$$

This approximation can be seen as the first step of a circular harmonic expansion of the renormalized dispersion $\epsilon(\mathbf{q})$ [4]. Since

$$\Gamma_k^{(2)}(\mathbf{q};\rho) = A_k \epsilon_0(\mathbf{q}) + U_k'(\rho) + 2\rho U_k''(\rho) \quad (40)$$

in a uniform field $\phi_{\mathbf{r}} = \sqrt{2\rho}$, we can define the renormalized spectrum amplitude by

$$A_k = \frac{1}{\epsilon_0}\Gamma_k^{(2)}(\mathbf{r}-\mathbf{r}';\rho_{0,k}) \quad (41)$$

where $\mathbf{r}$ and $\mathbf{r}'$ are nearest neighbors. The amplitude $A_k \equiv A_k(\rho_{0,k})$ should be understood as the first term in the expansion of the function

$$A_k(\rho) = A_k(\rho_{0,k}) + A_k^{(1)}(\rho_{0,k})(\rho - \rho_{0,k}) + \cdots \quad (42)$$

about the minimum $\rho_{0,k}$ of the effective potential $U_k(\rho)$. Another possible definition of the spectrum amplitude is $A_k \equiv A_k(\bar{\rho}_{0,k})$, where $\bar{\rho}_{0,k}$ is the minimum of $\bar{U}_k(\rho)$ [Eq. (37)]. The flow equation for $A_k$ follows from Eqs. (8) and (41),

$$\partial_k A_k = \frac{\gamma_3^2}{\epsilon_0}\int_{\mathbf{q}}\left(1 - \frac{\epsilon_0(\mathbf{q})}{2d\epsilon_0}\right)\partial_k R_k(\mathbf{q}) G(\mathbf{q})^2$$

$$\times \int_{\mathbf{p}}\left(1 - \frac{\epsilon_0(\mathbf{p})}{2d\epsilon_0}\right)G(\mathbf{p}), \quad (43)$$

where $\gamma_3 = \sqrt{2\rho_{0,k}}[3U_k''(\rho_{0,k}) + 2\rho_{0,k}U_k'''(\rho_{0,k})]$. The flow equa-
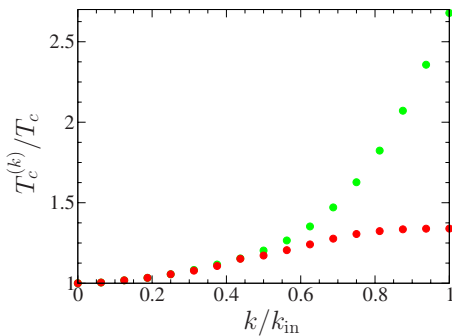


FIG. 5. (Color online) Transition temperature $T_c^{(k)}$ obtained from the effective potential $U_k$ (green points) and $\bar{U}_k$ (red points).
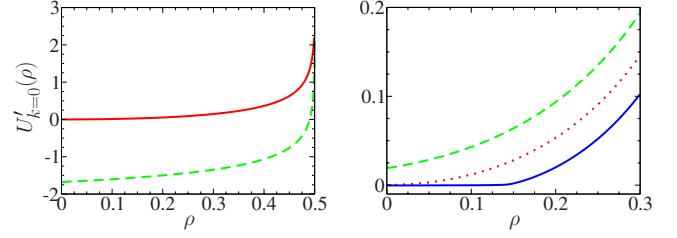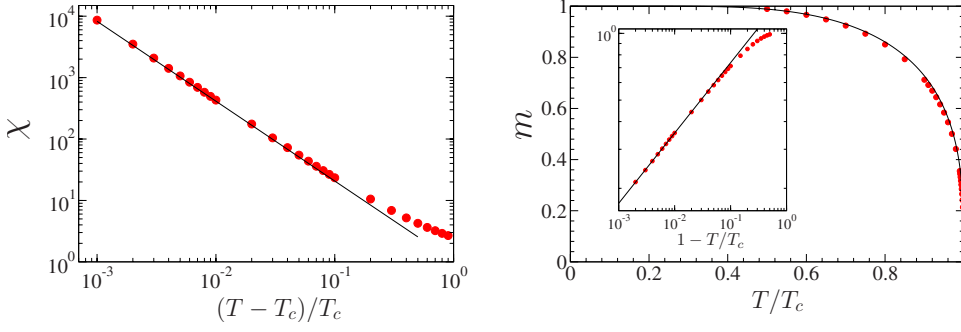
FIG. 7. (Color online) Left panel: uniform susceptibility $\chi$ (red points) in the high-temperature phase and a fit $\chi \propto (T-T_c)^{-\gamma}$ with $\gamma = 2\nu \simeq 1.30$. Right panel: magnetization $m$ in the low-temperature phase (red points) and the Essam-Fisher approximant [24] (solid line). The inset shows a fit to $m \propto (T_c - T)^\beta$ with $\beta = \nu/2 \simeq 0.32$.

tion for $U_k(\rho)$ is identical to Eq. (21) with $\epsilon_0(\mathbf{q})$ replaced by $A_k \epsilon_0(\mathbf{q})$.

Numerical results for $A_k(\rho_{0,k})$ and $A_k(\bar{\rho}_{0,k})$ are shown in Fig. 8. In both cases, $A_k$ varies when $k \sim 1$, in agreement with the expectation that the amplitude of the harmonic $\cos(nq_\nu)$ should vary when $k \sim 1/n$ [4]. The variation of $A_k$ is moderate [from 1 to 1.27 for $A_k(\rho_{0,k})$ and from 1 to 1.19 for $A_k(\bar{\rho}_{0,k})$] and weakly affects the critical temperature which remains within a few percents of the exact result: $T_c = 0.74 T_c^{\mathrm{MF}}$ with $A_k(\rho_{0,k})$ and $T_c = 0.72 T_c^{\mathrm{MF}}$ with $A_k(\bar{\rho}_{0,k})$. We expect that the inclusion of additional higher-order harmonics in the spectrum would give a better estimate of $T_c$.

### C. LPA′

When $k \ll 1$, we can approximate $\epsilon_0(\mathbf{q})$ by $\epsilon_0 \mathbf{q}^2$. In this regime, a simple improvement over the LPA (known as the LPA′) consists in including a field renormalization factor $Z_k$ so that the renormalized dispersion $\epsilon(\mathbf{q})$ is given by $Z_k \epsilon_0(\mathbf{q}) \simeq Z_k \epsilon_0 \mathbf{q}^2$. The LPA′ can be generalized to all values of $k$ by writing the average effective action as [4]

$$\Gamma_k[m] = \sum_\mathbf{r} U_k(\rho_\mathbf{r}) + \frac{1}{2} \sum_\mathbf{q} m_{-\mathbf{q}} Z_k \epsilon_0(\mathbf{q}) m_\mathbf{q}. \qquad (44)$$

Although this ansatz is formally similar to Eq. (39), $Z_k$ should not be confused with the amplitude $A_k$ introduced in Sec. III A. $Z_k$ is computed from the $\mathcal{O}(\mathbf{q}^2)$ part of the spectrum,

$$Z_k = \frac{1}{\epsilon_0} \lim_{\mathbf{q} \to 0} \frac{\partial}{\partial \mathbf{q}^2} \Gamma_k^{(2)}(\mathbf{q}; \rho_{0,k}), \qquad (45)$$

and therefore receives contributions from all harmonics. The LPA′ can be justified when $k \sim 1$ by noting that in this limit the renormalization of the spectrum is weak ($Z_k \sim 1$), so that the approximation $\epsilon(\mathbf{q}) \simeq Z_k \epsilon_0(\mathbf{q})$, valid for small $\mathbf{q}$, is expected to remain approximately valid in the whole Brillouin zone [4]. Nevertheless, because short-range fluctuations are important for the thermodynamics (Sec. III A), the LPA′ might lead to a slight deterioration of the value of $T_c$ obtained in the LPA. As in Sec. III A, we can compute $Z_k$ either from the minimum of $U_k(\rho)$ [as in Eq. (45)] or from the minimum $\bar{\rho}_{0,k}$ of $\bar{U}_k(\rho)$.

To obtain a fixed point when the system is critical, one should redefine the cutoff function,

$$R_k(\mathbf{q}) = Z_k[\epsilon_k - \epsilon_0(\mathbf{q})]\theta[\epsilon_k - \epsilon_0(\mathbf{q})], \qquad (46)$$

and introduce the dimensionless variables

$$\tilde{\rho} = Z_k k^{-d} \epsilon_k \rho, \qquad \tilde{U}_k(\tilde{\rho}) = k^{-d} U_k(\rho). \qquad (47)$$

This change of variables cannot be done at the beginning of the flow if one works with a given range of $\tilde{\rho}$ values. This would indeed correspond to a smaller and smaller range in $\rho$, whereas a good determination of the critical temperature requires to consider the window $0 \leq \rho \leq 1/2$. To circumvent this difficulty, we define

$$\tilde{\rho} = Z_k k^{-d} \epsilon_k g_1(k) \rho, \qquad \tilde{U}_k(\tilde{\rho}) = k^{-d} g_2(k) U_k(\rho), \qquad (48)$$

where

$$g_1(k) = \begin{cases} k^d (Z_k \epsilon_k)^{-1} & \text{if } k \gg k_c \\ 1 & \text{if } k \ll k_c, \end{cases}$$

$$g_2(k) = \begin{cases} k^d & \text{if } k \gg k_c \\ 1 & \text{if } k \ll k_c. \end{cases} \qquad (49)$$

For $k \gg k_c$, $\tilde{\rho}$ and $\tilde{U}_k$ are equal to $\rho$ and $U_k$, whereas they coincide with the dimensionless variables in Eq. (47) when $k \ll k_c$. The momentum scale $k_c$ will be determined below. In practice, we take

$$g_1(k) = [x + k^{-d} Z_k \epsilon_k (1-x)]^{-1},$$

$$g_2(k) = [x + k^{-d}(1-x)]^{-1}, \qquad (50)$$

where $x = e^{-(k/k_c)^n}$ with $n > d$. The parameter $n$ fixes the size of the crossover region $k \sim k_c$ between dimensionful and dimensionless variables (Fig. 9).

Figure 10 shows the RG time $-\tau(\rho)$ beyond which the potential $U_k'(\rho)$ differs from $U_{k=0}'(\rho)$ by less than $10^{-3}(d=3)$. (The RG time $t$ is defined by $k = k_{\mathrm{in}} e^t$.) This pre-
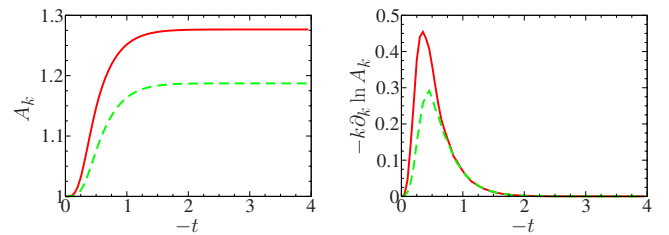


FIG. 8. (Color online) Left panel: $A_k(\rho_{0,k})$ (red solid line) and $A_k(\bar{\rho}_{0,k})$ (green dashed line) vs $-t = \ln(k_{\mathrm{in}}/k)$. Right panel: $-k\partial_k \ln A_k(\rho_{0,k})$ (red solid line) and $-k\partial_k \ln A_k(\bar{\rho}_{0,k})$ (green dashed line) vs $-t$. All curves are obtained at criticality ($T = T_c$) and for $d = 3$.
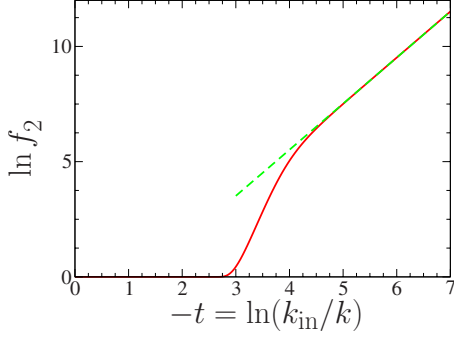
FIG. 9. (Color online) The function $f_2(k)=k^{-d}g_2(k)$ vs $-t=-\ln(k/k_{\rm in})$ for $n=6$ and $t_c=-3$ $(d=2)$. The green dashed line corresponds to $g_2(k)=1$.

cision $(10^{-3})$ is sufficient to determine the critical temperature to an accuracy on the order of 1%. As expected, the potential converges to its asymptotic value faster for large values of $\rho$. In Fig. 10, the red solid line shows the maximum value $\rho_{\rm max}=\frac{1}{2}e^\tau$ at time $\tau$ if one works with a fixed window $\tilde\rho\in[0,1/2]$ [Eq. (47)] (we neglect $Z_{k=e^\tau}\simeq1$ in the calculation of $\rho_{\rm max}$). Thus, we see that a natural choice for $t_c=\ln(k_c/k_{\rm in})$ is $t_c\simeq-2.5$ since for times $-t>-t_c$ the window $[0,\rho_{\rm max}]$ becomes larger than the range of $\rho$ values for which the potential $U'_k(\rho)$ has not converged to its asymptotic value yet. In practice, we verify that our results are independent of the precise choice of $k_c$ and $n$.

The change of variables in Eq. (48) leads to the flow equations

$$k\partial_k\tilde U_k=\left(-d+\frac{k\partial_k g_2}{g_2}\right)\tilde U_k+\left(d-2+\eta_k-\frac{k\partial_k g_1}{g_1}\right)\tilde\rho\tilde U'_k$$
$$+\frac{g_2}{1+\frac{g_1}{g_2}(\tilde U'_k+2\tilde\rho\tilde U''_k)}[(2-\eta_k)I_1+\eta_k I_2]\quad(51)$$

and

$$\eta_k=4\frac{g_1^3}{g_2^2}\tilde\rho[3\tilde U''_k+2\tilde\rho\tilde U'''_k]^2\frac{I_3+\delta_{d,2}/(8\pi)}{\left[1+\frac{g_1}{g_2}(\tilde U'_k+2\tilde\rho\tilde U''_k)\right]^4},\quad(52)$$
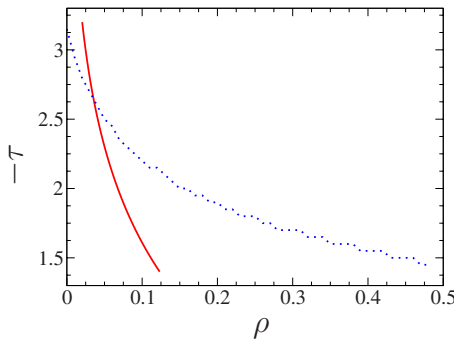
where



FIG. 10. (Color online) RG time $-\tau(\rho)$ beyond which the potential $U'_k(\rho)$ differs from $U'_{k=0}(\rho)$ by less then $10^{-3}$ (blue dotted line). The red solid line shows $\rho=\frac{1}{2}e^\tau$ (see text).
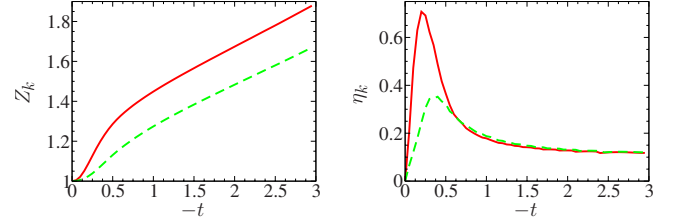


FIG. 11. (Color online) Left panel: $Z_k$ vs $-t=\ln(k_{\rm in}/k)$ obtained with $\rho_{0,k}$ (red solid line) and $\bar\rho_{0,k}$ (green dashed line) $(d=3)$. Right panel: anomalous dimension $\eta_k=-k\partial_k\ln Z_k$ obtained with $\rho_{0,k}$ (red solid line) and $\bar\rho_{0,k}$ (green dashed line).

$$I_1=\frac{k^{-d}}{2}\int_{\mathbf q}\theta[\epsilon_k-\epsilon_0(\mathbf q)],$$

$$I_2=\frac{k^{-d}}{2}\int_{\mathbf q}\frac{\epsilon_0(\mathbf q)}{\epsilon_k}\theta[\epsilon_k-\epsilon_0(\mathbf q)],$$

$$I_3=\frac{k^{2-d}}{4}\int_{\mathbf q}\frac{\epsilon_0(\mathbf q)\partial_{q_x}^2\epsilon_0(\mathbf q)-[\partial_{q_x}\epsilon_0(\mathbf q)]^2}{\epsilon_0(\mathbf q)^2}\theta[\epsilon_k-\epsilon_0(\mathbf q)]$$
$$(53)$$

(see the Appendix). In Eq. (52), the right-hand side should be evaluated at $\tilde\rho_{0,k}$ or $\tilde{\bar\rho}_{0,k}$. For $d=3$ and $n>3$, the numerical solution of the flow Eqs. (51) and (52) is stable for $-t_c\gtrsim2$. The results described below are obtained for $n=4$ and $t_c=-3$. We find $T_c=0.8T_c^{\rm MF}$ when $Z_k$ is defined with respect to the minimum $\rho_{0,k}$ of $U_k$, and $T_c=0.74T_c^{\rm MF}$ if we use the minimum $\bar\rho_{0,k}$ of $\bar U_k$. The result is not as accurate as in the LPA [as anticipated above; see the discussion following Eq. (45)]. Nevertheless, with $\bar\rho_{0,k}$ (the only case we discuss in the following), it remains within 2% of the exact result $T_c^{\rm exact}=0.752T_c^{\rm MF}$. The flow of $Z_k$ is shown in Fig. 11. For $-t<1$, $Z_k$ does not differ significantly from $A_k$ (Fig. 8). In this regime, only the first harmonic (i.e., $\cos q_\nu$) is expected to vary and therefore contribute to $Z_k$. For $-t>1$, the renormalization of higher-order harmonics makes $Z_k$ deviate from $A_k$. While $A_k$ saturates to $\sim1.19$, $Z_k\sim k^{-\eta^*}$ diverges with an exponent given by the anomalous dimension $\eta^*=\lim_{k\to0}\eta_k$. $\eta^*\simeq0.1$ is a poor estimate of the exact result $\eta^*\simeq0.036$ but agrees with previous estimates based on the LPA' [4]. A $\rho$ dependence of $Z_k$ is expected to improve the value of $\eta^*$ [27].

### D. Comparison with HRT

Our approach bears similarities with the hierarchical reference theory (HRT) of fluids [28–32] (for a review, see Ref. [13]). The HRT is based on an exact treatment of short-distance (hard-core) interactions supplemented by a RG analysis of long-range interactions. The HRT also applies to classical spin models: as in the lattice NPRG, it starts from the local theory (decoupled sites) and takes into account the intersite coupling in a RG approach. Although the final results are very similar to those we have obtained in Secs. III A

and III B, the HRT nevertheless differs from the lattice NPRG in some technical aspects, e.g., the choice of the cut-off function and the way degrees of freedom are progressively integrated out [13,33]. Because it was first developed in the context of liquid state theory, the connection between HRT and the more standard formulation of the NPRG [2] is not always obvious (for a discussion of the relation between HRT and RG; see Refs. [34,35]). By contrast, the lattice NPRG is formulated in the usual language of statistical field theory. The various improvements over the LPA known for continuum models can then be easily implemented in the lattice NPRG. In Sec. III C, we have discussed one of these improvements, the LPA′, which allows us to compute the anomalous dimension $\eta$.

## IV. BKT TRANSITION IN 2D *XY* MODEL

The NPRG approach to the continuum O(2) (linear) model reproduces most of the universal properties of the BKT transition in two dimensions [36,37]. In particular, one finds a value $\tilde{\rho}_0^*$ of the dimensionless order parameter (the spin-wave "stiffness") such that the $\beta$ function $\beta(\tilde{\rho}_{0,k}) = k\partial_k\tilde{\rho}_{0,k}$ nearly vanishes for $\tilde{\rho}_{0,k} > \tilde{\rho}_0^*$, which reflects the existence of a line of quasifixed points. In this low-temperature phase, after a transient regime, the running of the stiffness $\tilde{\rho}_{0,k}$ becomes very slow, which implies a very large, although not strictly infinite, correlation length $\xi$. The anomalous dimension $\eta_k$ depends on the (slowly varying) stiffness and takes its largest value when the system crosses over to the disordered regime ($\tilde{\rho}_{0,k} \sim \tilde{\rho}_0^*$ and $k \sim \xi^{-1}$). When $\tilde{\rho}_{0,k} < \tilde{\rho}_0^*$, the essential scaling $\xi \sim e^{a/(\tilde{\rho}_0^* - \tilde{\rho}_{0,k})^{1/2}}$ of the correlation length is reproduced [37].

In this section, we apply the lattice NPRG to the two-dimensional *XY* model defined by the Hamiltonian

$$H = -\frac{J}{T}\sum_{\langle \mathbf{r},\mathbf{r}'\rangle} \mathbf{S}_{\mathbf{r}} \cdot \mathbf{S}_{\mathbf{r}'}, \tag{54}$$

where $\mathbf{S}_{\mathbf{r}} = (\cos\theta_{\mathbf{r}}, \sin\theta_{\mathbf{r}})$ is a 2D classical spin of unit length. Up to a multiplicative constant, the initial value of the partition function $Z_{k_{\text{in}}}[\mathbf{h}] = \Pi_{\mathbf{r}}\, z(h_{\mathbf{r}})(h_{\mathbf{r}} = |\mathbf{h}_{\mathbf{r}}|)$ is determined by the partition function of a single site,

$$z(h) = \int_0^{2\pi}\frac{d\theta}{2\pi}e^{h\cos\theta} = I_0(h). \tag{55}$$

The magnetization points along the applied field with an amplitude

$$m(h) = \frac{\partial}{\partial h}\ln z(h) = \frac{I_1(h)}{I_0(h)}, \tag{56}$$

where $I_0(h)$ and $I_1(h)$ are modified Bessel functions. Contrary to the Ising model, the function $h(m)$ obtained by inverting Eq. (56) must be computed numerically. For $k = k_{\text{in}}$ the average effective action takes the form

$$\Gamma_{k_{\text{in}}}[\mathbf{m}] = \sum_{\mathbf{r}} U_{k_{\text{in}}}(\rho_{\mathbf{r}}) + \frac{1}{2}\sum_{\mathbf{q}}\epsilon_0(\mathbf{q})\mathbf{m}_{-\mathbf{q}}\cdot\mathbf{m}_{\mathbf{q}} \tag{57}$$

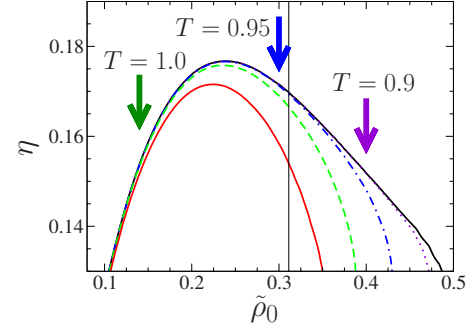($\rho_r = \mathbf{m}_{\mathbf{r}}^2/2$), with



FIG. 12. (Color online) Flow trajectories $(\tilde{\rho}_0, \eta)$ for the two-dimensional *XY* model. $T_c/J = 1.05$ (red solid line), 1 (green dashed line), 0.95 (blue dash-dotted line), 0.9 (dotted purple line), and 0.85 (black solid line). The arrows indicate the merging points with the line of quasifixed points. The vertical line shows the value of $\tilde{\rho}_0^*$.

$$U_{k_{\text{in}}}(\rho) = -\ln z(h) + h\sqrt{2\rho} - 8\epsilon_0\rho. \tag{58}$$

Expanding $I_0(h)$ and $I_1(h)$ for small $h$, one finds $m = h/2 + \mathcal{O}(h^3)$ and in turn

$$U_{k_{\text{in}}}(\rho) = 2\rho(1 - 4\epsilon_0) + \mathcal{O}(\rho^2). \tag{59}$$

This yields the transition temperature $T_c^{(k_{\text{in}})} = 4J$, which differs from the mean-field result $T_c^{\text{MF}} = 2J$ for reasons explained in Sec. III.

In the LPA′, the flow equations read

$$k\partial_k\tilde{U}_k = \left(-2 + \frac{k\partial_k g_2}{g_2}\right)\tilde{U}_k + \left(\eta_k - \frac{k\partial_k g_1}{g_1}\right)\tilde{\rho}\tilde{U}_k'$$
$$+ \left(\frac{g_2}{1 + \frac{g_1}{g_2}(\tilde{U}_k' + 2\tilde{\rho}\tilde{U}_k'')} + \frac{g_2}{1 + \frac{g_1}{g_2}\tilde{U}_k'}\right)$$
$$\times[(2 - \eta_k)I_1 + \eta_k I_2] \tag{60}$$

and

$$\eta_k = 8\frac{g_1^3}{g_2^2}\tilde{\rho}(U_k'')^2\left[1 + \frac{g_1}{g_2}(\tilde{U}_k' + 2\tilde{\rho}\tilde{U}_k'')\right]^{-2}\left[1 + \frac{g_1}{g_2}\tilde{U}_k'\right]^{-2}$$
$$\times\left(I_3 + \frac{1}{8\pi}\right), \tag{61}$$

where we evaluate the right-hand side in Eq. (61) at the minimum (which we denote by $\tilde{\rho}_{0,k}$ for simplicity) of the potential $\tilde{\bar{U}}_k(\tilde{\rho})$ [Eq. (37)] (see the Appendix). $I_1$, $I_2$, and $I_3$ are defined in Eq. (53). We use the change of variables in Eq. (48) with $n = 3$ and $t_c = -2$.

The flow trajectories in the plane $(\tilde{\rho}_0, \eta)$ are shown in Fig. 12. The flow diagram is reminiscent of the results obtained in the continuum 2D O(2) model [36,37]. At low temperature ($T \lesssim J$), the trajectories join a line of quasifixed points. The value of $\tilde{\rho}_0$ at the merging point depends on the temperature. The critical temperature of the BKT transition is defined by the trajectory for which the merging point corresponds to $\tilde{\rho}_0^*$. A precise determination of the value of $\tilde{\rho}_0^*$ [which can be obtained by fitting the beta function $k\partial_k\tilde{\rho}_{0,k}$ to $\frac{1}{\nu}(\tilde{\rho}_{0,k} - \tilde{\rho}_0^*)^{3/2}$] is however not possible in the LPA′ as it requires the full

$\mathcal{O}(\partial^2)$ expansion of the effective action in the continuum limit $k \ll 1$ [37]. Since for the long-distance properties of the *XY* model the lattice should not matter, we make the assumption that the ratio $\tilde{\rho}_0^* / \tilde{\rho}_{max}$ ($\tilde{\rho}_{max}$ is the value of $\tilde{\rho}_0$ for which $\eta$ is maximum) takes the same value in the *XY* and continuum O(2) models. We can then deduce the value of $\tilde{\rho}_0^*$ from the results in Ref. [37]. Although this determination of $T_c$ is clearly approximate, we can nevertheless conclude from our results that $0.9 < T_c/J < 1$. This estimate should be compared to the exact result $T_c^{exact} = 0.89J$ obtained from the Monte Carlo calculations [38] and the mean-field expression $T_c^{MF} = 2J$. Note that the relative error on $T_c$ is of the same order of magnitude as in the 2D Ising model (Sec. III A).

## V. CONCLUSION

We have proposed an implementation of the NPRG, which takes as a reference system the local limit of decoupled sites rather than a system where fluctuations are frozen. The lattice NPRG captures both local and critical fluctuations in a nontrivial way. For a lattice field theory and classical spin models, the LPA is sufficient to compute nonuniversal quantities (transition temperature and magnetization) to an accuracy on the order of 1%. We have also discussed an approximation (the LPA$'$) which goes beyond the LPA and allows us to compute the anomalous dimension $\eta$.

A new NPRG scheme has been recently proposed by Blaizot, Méndez-Galain, and Wschebor (BMW) [39,40]. The BMW approach relies on approximate flow equations for the effective potential $U_k$ and the two-point vertex $\Gamma_k^{(2)}$. Contrary to the LPA and the LPA$'$, it keeps the full momentum dependence of the two-point vertex. We believe that the BMW scheme provides the natural framework to go beyond the LPA in the lattice NPRG.

There are many theoretical methods where the idea to use a reference system which includes short-range fluctuations is central. These methods are usually based on "cluster" approaches where one solves exactly (usually numerically) the model on a single cluster (possibly a single site) [41] and includes the coupling between clusters by means of a perturbative calculation, a self-consistent condition, etc. The cluster approaches include the correlated cluster mean-field theory in classical spin models (see, e.g., Ref. [42] and references therein), the dynamical mean-field theory [43,44] (DMFT) and its extensions (cellular DMFT [45,46]), the cluster perturbation theory [47,48], the variational cluster approach [49], and the self-energy functional theory [50]. These approaches describe exactly the local fluctuations but struggle to take into account low-energy (collective) fluctuations which become very important near a phase transition or in low dimensions.

In this context the lattice NPRG may be seen as a step toward a theory including both local and critical fluctuations in strongly correlated systems. While we have only discussed classical models, the lattice NPRG can be easily applied to interacting boson systems (the Bose-Hubbard model) [51].

## APPENDIX: ANOMALOUS DIMENSION

In this appendix, we compute the anomalous dimension for the Ising model. From definition (45) and flow equation (8), one obtains the following expression of the (running) anomalous dimension $\eta_k = -k\partial_k \ln Z_k$,

$$\eta_k = \frac{\gamma_3^2}{2Z_k\epsilon_0} \int_{\mathbf{q}} \partial_{q_x} G_k(\mathbf{q}) \partial_{q_x} [k\partial_k R_k(\mathbf{q}) G_k(\mathbf{q})^2], \quad (A1)$$

where $\gamma_3$ is defined after Eq. (43). To proceed further, we use

$$R = Z\epsilon_k y r,$$

$$k\partial_k R = -(\eta r + 2yr')Z\epsilon_k y,$$

$$\partial_{q_x} R = Z(r + yr')\partial_{q_x}\epsilon,$$

$$\partial_{q_x} k\partial_k R = -Z[\eta_k r + (\eta+4)yr' + 2y^2 r'']\partial_{q_x}\epsilon,$$

$$\partial_{q_x} G = -G^2 Z(1 + r + yr')\partial_{q_x}\epsilon, \quad (A2)$$

where $r \equiv r(y) = \theta(1-y)(1-y)/y$, $\epsilon \equiv \epsilon_0(\mathbf{q})$, $G \equiv G(\mathbf{q})$, and $y = \epsilon/\epsilon_k$. To alleviate the notations we now drop the $k$ index. The product of $\partial_{q_x} G \propto (1 + r + yr') = \theta(y-1)$ and $\partial_{q_x} k\partial_k R$ gives zero except for possible singular contributions at $y = 1$ coming from $r''r$ and $r''r'$. Thus, Eq. (A1) simplifies into

$$\eta = \frac{Z\gamma_3^2}{\epsilon_0} \int_{\mathbf{q}} y^2 r''(1 + r + yr') G^4 (\partial_{q_x}\epsilon)^2. \quad (A3)$$

By an integration by part we obtain

$$\int_{\mathbf{q}} y^2 r''(1+r) G^4 (\partial_{q_x}\epsilon)^2$$

$$= \epsilon_k \int_{\mathbf{q}} y^2 (1+r) G^4 \partial_{q_x}\epsilon \partial_{q_x} r'$$

$$= -\epsilon_k \int_\mu^\pi \frac{dq_x}{\pi} \int_{\mathbf{q}_\perp} \theta(\mathbf{q}_\perp^2 - \mu^2) r' \partial_{q_x} [y^2(1+r) G^4 (\partial_{q_x}\epsilon)^2]$$

$$+ \frac{\epsilon_k}{\pi} \int_{\mathbf{q}_\perp} \theta(\mathbf{q}_\perp^2 - \mu^2) y^2(1+r) G^4 (\partial_{q_x}\epsilon) r'|_{q_x=\mu}^{q_x=\pi}, \quad (A4)$$

where $\mathbf{q}_\perp = (q_y, q_z, \ldots)$. Note that we have regularized the integrals near $\mathbf{q} = 0$ ($\mu \to 0^+$). To compute the first integral in Eq. (A4), $I_1$, we remark that if $\partial_{q_x}$ acts on $G^4$ then the integrand vanishes, so that

$$I_1 = \frac{\bar{G}^4}{(Z\epsilon_k)^4} \int_{\mathbf{q}} \frac{\theta(1-y)}{y^2} [\epsilon(\partial_{q_x}^2\epsilon) + (\partial_{q_x}\epsilon)^2], \quad (A5)$$

where $\bar{G} = Z\epsilon_k/[Z\epsilon_k + U'(\rho_0) + 2\rho_0 U''(\rho_0)]$. The second contribution in Eq. (A4) reads

$$I_1' = \frac{\bar{G}^4}{\pi Z^4 \epsilon_k^3} \int_{\mathbf{q}_\perp} \theta(\mathbf{q}_\perp^2 - \mu^2) \frac{\theta(1-y)}{y} (\partial_{q_x} \epsilon)|_{q_x=\mu}, \quad (A6)$$

since $\partial_{q_x} \epsilon = 2\epsilon_0 \sin(q_x)$ vanishes for $q_x = \pi$. For $\mu \to 0^+$, we obtain

$$I_1' = \frac{2\bar{G}^4}{\pi Z^4 \epsilon_k^2} \int_{\mathbf{q}_\perp} \theta(\mathbf{q}_\perp^2 - \mu^2) \theta(1-y) \frac{\mu}{\mathbf{q}_\perp^2 + \mu^2}, \quad (A7)$$

where the Lorentzian $\mu/(\mathbf{q}_\perp^2 + \mu^2)$ acts as a delta function $\sim \delta(q_\perp)$. Thus, the integral vanishes for $d > 2$ and takes the value $\bar{G}^4/(2\pi Z^4 \epsilon_k^2)$ for $d = 2$. By a similar reasoning, we find

$$\int_{\mathbf{q}} y^3 r'' r' G^4 (\partial_{q_x} \epsilon)^2 = -\frac{\bar{G}^4}{2(Z\epsilon_k)^4} \int_{\mathbf{q}} \frac{\theta(1-y)}{y^2}$$

$$\times [\epsilon(\partial_{q_x}^2 \epsilon) + 3(\partial_{q_x} \epsilon)^2] - \frac{1}{2} I_1'. \quad (A8)$$

We deduce

$$\eta = \frac{\gamma_3^2 \bar{G}^4}{2\epsilon_0 Z^3 \epsilon_k^2} \left\{ \int_{\mathbf{q}} \frac{\theta(\epsilon_k - \epsilon)}{\epsilon^2} [\epsilon(\partial_{q_x}^2 \epsilon) - (\partial_{q_x} \epsilon)^2] + \frac{\delta_{d,2}}{2\pi} \right\}. \quad (A9)$$

In the continuum limit, one recovers the known results of the LPA′. In particular, when $U(\rho) = \frac{\lambda}{2}(\rho - \rho_0)^2$ is truncated to second order in $\rho$,

$$\eta = 72 \frac{v_d}{d} \frac{\tilde{\rho}_0 \tilde{\lambda}^2}{(1 + 2\tilde{\rho}_0 \tilde{\lambda})^4}. \quad (A10)$$

Note that the last term in Eq. (A9) ensures that $\eta$ is a continuous function of $d$. For the *XY* model, a similar calculation leads to Eq. (61).

[1] C. Wetterich, Phys. Lett. B **301**, 90 (1993).
[2] J. Berges, N. Tetradis, and C. Wetterich, Phys. Rep. **363**, 223 (2002).
[3] B. Delamotte, e-print arXiv:cond-mat/0702365.
[4] N. Dupuis and K. Sengupta, Eur. Phys. J. B **66**, 271 (2008).
[5] C. Wetterich, Phys. Rev. B **77**, 064504 (2008).
[6] S. Floerchinger and C. Wetterich, Phys. Rev. A **77**, 053603 (2008).
[7] N. Dupuis and K. Sengupta, EPL **80**, 50007 (2007).
[8] N. Dupuis, Phys. Rev. Lett. **102**, 190401 (2009).
[9] N. Dupuis, Phys. Rev. A **80**, 043627 (2009).
[10] A. Sinner, N. Hasselmann, and P. Kopietz, Phys. Rev. Lett. **102**, 120601 (2009).
[11] A. Sinner, N. Hasselmann, and P. Kopietz, e-print arXiv:1008.4521.
[12] L. P. Kadanoff, Physics (Long Island City, N.Y.) **2**, 263 (1966).
[13] A. Parola and L. Reatto, Adv. Phys. **44**, 211 (1995).
[14] V. L. Berezinskii, Sov. Phys. JETP **32**, 493 (1970); **34**, 610 (1971).
[15] J. M. Kosterlitz and D. J. Thouless, J. Phys. C **6**, 1181 (1973).
[16] D. Litim, Phys. Lett. B **486**, 92 (2000).
[17] *Stricto sensu*, the local limit of Hamiltonian (1) corresponds to $C = 0$.
[18] When $k \ll 1$, we can use $\epsilon_0(\mathbf{q}) \simeq \epsilon_0 \mathbf{q}^2$ and $\mathcal{D}(\epsilon) \simeq 2v_d \epsilon^{d/2-1}/\epsilon_0^{d/2}$, where $v_d^{-1} = 2^{d+1} \pi^{d/2} \Gamma(d/2)$. Equation (21) then reduces to the usual LPA equation derived in the continuum limit of model (1) [2].
[19] We omit a factor of $T$ in the definition of the susceptibility.
[20] U. Wolff, Phys. Lett. B **228**, 379 (1989).
[21] We use ln cosh argtanh $x = -\frac{1}{2}\ln(1-x^2)$.
[22] M. Hasenbusch and S. Meyer, Phys. Lett. B **241**, 238 (1990).
[23] C. Holm and W. Janke, Phys. Rev. B **48**, 936 (1993).
[24] J. W. Essam and M. E. Fisher, J. Chem. Phys. **38**, 802 (1963).
[25] C. Bervillier, B. Boisseau, and H. Giacomini, Nucl. Phys. B **789**, 525 (2008).
[26] L. Onsager, Phys. Rev. **65**, 117 (1944).
[27] L. Canet, B. Delamotte, D. Mouhanna, and J. Vidal, Phys. Rev. D **67**, 065004 (2003).
[28] A. Parola and L. Reatto, Phys. Rev. Lett. **53**, 2417 (1984).
[29] G. Gianinetti and A. Parola, Phys. Rev. B **63**, 104414 (2001).
[30] A. Parola, J. Phys. C **19**, 5071 (1986).
[31] C. D. Ionescu, A. Parola, D. Pini, and L. Reatto, Phys. Rev. E **76**, 031113 (2007).
[32] A. Parola, D. Pini, and L. Reatto, e-print arXiv:0901.2064.
[33] D. Pini, A. Parola, and L. Reatto, J. Stat. Phys. **72**, 1179 (1993).
[34] J. M. Caillol, Mol. Phys. **104**, 1931 (2006).
[35] J. M. Caillol, J. Phys. A **42**, 225004 (2009).
[36] M. Gräter and C. Wetterich, Phys. Rev. Lett. **75**, 378 (1995).
[37] G. v. Gersdorff and C. Wetterich, Phys. Rev. B **64**, 054513 (2001).
[38] P. Olsson, Phys. Rev. B **52**, 4526 (1995).
[39] J.-P. Blaizot, R. Méndez-Galain, and N. Wschebor, Phys. Lett. B **632**, 571 (2006).
[40] F. Benitez, J. P. Blaizot, H. Chaté, B. Delamotte, R. Méndez-Galain, and N. Wschebor, Phys. Rev. E **80**, 030103(R) (2009).
[41] Note that one could also take a system of decoupled clusters as the reference state in the lattice NPRG.
[42] D. Yamamoto, Phys. Rev. B **79**, 144427 (2009).
[43] W. Metzner and D. Vollhardt, Phys. Rev. Lett. **62**, 324 (1989).
[44] A. Georges, G. Kotliar, W. Krauth, and M. J. Rozenberg, Rev. Mod. Phys. **68**, 13 (1996).
[45] M. H. Hettler, A. N. Tahvildar-Zadeh, M. Jarrell, T. Pruschke, and H. R. Krishnamurthy, Phys. Rev. B **58**, R7475 (1998).
[46] G. Kotliar, S. Y. Savrasov, G. Pálsson, and G. Biroli, Phys. Rev. Lett. **87**, 186401 (2001).
[47] C. Gros and R. Valentí, Phys. Rev. B **48**, 418 (1993).
[48] D. Sénéchal, D. Pérez, and M. Pioro-Ladrière, Phys. Rev. Lett. **84**, 522 (2000).
[49] M. Potthoff, M. Aichhorn, and C. Dahnken, Phys. Rev. Lett. **91**, 206402 (2003).
[50] M. Potthoff, Eur. Phys. J. B **32**, 429 (2003).
[51] A. Rançon and N. Dupuis (unpublished).